24th COBEM - 2017

24th ABCM International Congress of Mechanical Engineering
December 3-8, 2017, Curitiba, PR, Brazil

COBEM-2017-0534
THE USE OF XFEM FOR STRESS INTENSITY FACTOR ESTIMATION OF SURFACE CRACKS

Gabriel de Castro Coêlho
Antonio Almeida Silva
Marco Antonio dos Santos
Federal University of Campina Grande - Aprigio Veloso Street, 882 – Bairro Universitário, Campina Grande, PB. CEP: 58429-900.
gabrielcastro_c90@hotmail.com

Neilor Cesar dos Santos
Federal Institut of Education, Science and Tecnology of Paraíba – Primeiro de Maio Avenue, 720 – Jaguaribe, João Pessoa, PB. CEP: 58015-435.
neilorcesar@gmail.com

Abstract. *The eXtended Finite Element Method (XFEM) is a numerical technique based on the Partition of the Unity Finite Element Method (PUFEM) that has overcome difficulties in the modelling of structures containing strong discontinuities, such as cracks, in comparison to the conventional Finite Element Method (FEM). The practical use of the XFEM for structural integrity assessment was evaluated in comparison with the conventional FEM for the extraction of the Stress Intensity Factor (SIF) of common engineering structures with surface semi elliptical cracks. The structures here considered were a plate and a hollow cylinder. Two types of model were considered for the hollow cylinder case: surface-based tie constraint model and complete model. Two types of mesh structuring technique around crack location were also considered both for the plate and hollow cylinder. Both FEM and XFEM models results were compared with common analytical solutions. Results indicate that the XFEM can be used as a reliable technique for SIF estimation, but attention should be taken specially to the mesh structure around crack location, which proved to be crucial to the agreement of the SIF profile obtained by this numerical technique to the analytical solution and FEM results.*

Keywords: *extended finite element method, stress intensity factor, surface semi elliptical crack, plate and hollow cylinder.*

1. INTRODUCTION

The use of the conventional Finite Element Method (FEM) in the fracture mechanics analysis has become a resourceful way for analysing structures containing cracks and for Stress Intensity Factor (SIF) estimation instead of the use of analytical solutions (sometimes hardworking to be practically applied). On the other hand, it also implies the necessity for the mesh to adapt to both component geometry and crack topology, what results in simplified models (Qian et al., 2016) that may not represent quite so well the real situation intended to be numerically analysed. In addition, finer mesh in the crack location is always required for better results.

Overcoming these disadvantages, Belytschko and Black (1999) introduced a method for numerical treatment of cracks without the need of the mesh adaptation to their topology with minimal remeshing by adding extra degrees of freedom at selected nodes. These selected nodes would represent the crack in that location on the discretized continuum by adding enrichment functions from the analytical solutions of the dislocation fields of a crack tip, the asymptotic functions; hence representing the crack singularity. The method was then improved by Möes, Dolbow and Belytschko (1999) with the addition of more degrees of freedom through discontinuous fields across the crack faces away from its tips, the Haar ("jump") functions. This method was then called the eXtended Finite Element Method (XFEM) and has become an advance in element technology for it allows strong discontinuities to be arbitrarily represented by cutting elements (Sukumar, Dolbow and Moës, 2015) as shown in Fig. 1 in comparison with the FEM approach.

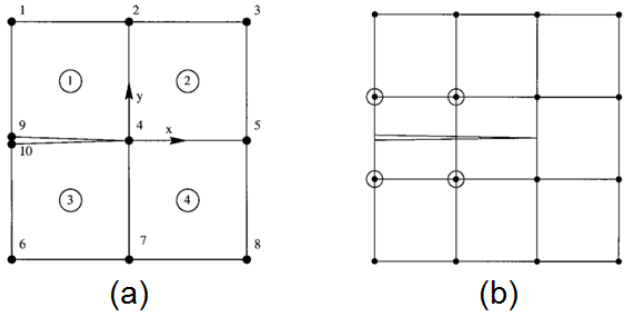

Figure 1. Comparison of the approaches for numerical evaluation of a crack by (a) FEM; (b) XFEM. Adapted from Möes, Dolbow and Belytschko (1999).

The XFEM makes use of the Partition of the Unity Finite Element Method (PUFEM) introduced by Melenk and Babuška (1996) whose one of the applications is to allow the user to include prior knowledge about singularities perturbed under consideration in the finite element space. The discretization in one dimension performed by the XFEM is (Möes, Dolbow and Belytschko, 1999):

$$\mathrm{u}^{\mathrm{h}} = \sum_{i \in I} u_i \phi_i + \sum_{j \in J} b_j \phi_j H(x) + \sum_{k \in K} \phi_k [\sum_{l=1}^{4} c_k^l F_l(x)] \tag{1}$$

where u is the degree of freedom at a node $i \in I$; b is the degree of freedom at a node $j \in J$ through where the crack lies; c the degree of freedom at a node $k \in K$ that contain the crack tip; ϕ is the shape function defined at the node; $H(x)$ are the Haar functions; $F_l(x)$ are the asymptotic functions; I is the set of all nodes of the mesh; J is the set of nodes such that $J \in I$ where the crack lies; and K is the set of nodes such that $K \in I$ where the crack tip lies.

The Haar functions enriches the discretization by introducing the relative location of the crack to a reference point (RP), indicating if this point is above or below the crack and it is given by (Möes; Dolbow; Belytschko, 1999):

$$H(x,y) = \begin{cases} 1, \text{if the crack is above RP} \\ -1, \text{if the crack is below RP} \\ 0, \text{if the crack lies on RP} \end{cases} \tag{2}$$

The asymptotic functions are the same as the ones developed by Fleming et al. (1997):

$$F_l(r,\theta) = \left\{ \sqrt{r}\sin\left(\frac{\theta}{2}\right), \sqrt{r}\cos\left(\frac{\theta}{2}\right), \sqrt{r}\sin\left(\frac{\theta}{2}\right)\sin(\theta), \sqrt{r}\cos\left(\frac{\theta}{2}\right)\sin(\theta) \right\} \tag{3}$$

where r, θ are the polar coordinates at the crack tip. The first function in equation (3) is the only one out of the others that represents the discontinuity across the crack faces (Möes; Dolbow and Belytschko, 1999; Sukumar et al., 2000).

The XFEM has been intensively used for crack growth analysis, as it does not require mesh refinement at each crack dimension increment. The XFEM has also been used for SIF estimation, as it requires only the use of linear elements instead of quadratic elements required by FEM, what reduces computational cost greatly. The assessment concerning the comparison to FEM and XFEM models of structures containing crack-like flaws is indeed of very importance, because a more precise estimation might make a great impact on structural integrity assessment procedures.

The objective of this paper is to assess the capability of the XFEM for SIF estimation in comparison with the conventional FEM for two structures geometries: a plate and a hollow cylinder.

2. COMPUTATIONAL PROCEDURE

Commercial software ABAQUS® will be used for the modelling of the structures where a surface crack with semi elliptical shape will be modelled so that the loading mode I SIF, K_I, can be extracted through both XFEM and FEM. The analysis will take place into the field of the linear elastic fracture mechanics, as the XFEM is only implemented in ABAQUS® for linear elastic materials. A structural steel will be considered with Young's modulus of 207 GPa and Poisson's ratio of 0.33.

The common engineering structures to be assessed are a plate and a hollow cylinder. Tab. 1 summarizes each structure with its dimension, crack location and crack dimension. The plate is characterized by its height (h), width (w) and thickness (t), while the hollow cylinder is characterized by its internal radius (R_i), thickness and width. The surface crack is characterized as shown in Fig. 2.

Table 1 – Structures to be modelled and each of their crack dimensions.

Structures	**Dimension values [mm]**	**Surface crack dimensions [mm]**		**Crack location**
		2c	**a**	
Plate	h x w x t 20 x 10 x 1	2	0.5	Centered at the face defined by 20 x 10 mm
Hollow cylinder	R_i x t x w 200 x 20 x 300	16	4	Outside surface, axial direction

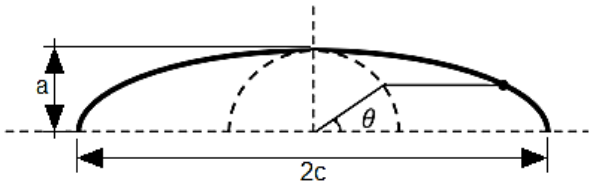

Figure 2. Characterization of a surface crack with semi elliptical shape. Adapted from Levén and Rickert (2012).

The angle θ is called parametric angle and the SIF profile will be calculated along it. For both geometries, full model will be developed but the SIF profile will be extracted only for half the parametric angle interval ($0 \leq \theta \leq 90°$), because of the SIF profile symmetry at $\theta = 90°$. The SIF profiles obtained will be normalized as:

$$K_I^{norm} = \frac{K_I}{\sigma\sqrt{(\pi a)}} \tag{4}$$

where K_I^{norm} is the normalized mode I SIF value and σ is the primary load remotely inducing mode I stress case on the structure.

The results of both XFEM and FEM analysis will be explicitly checked with typical analytical solutions available in the literature. The solutions for both geometries are given by BS 7910 (2013) standard. The plate solution is derived from Newman and Raju (1984) and is used with few geometry parameters modifications for the hollow cylinder solution. The plate will be submitted to a remote tension of 100 MPa and the hollow cylinder will be submitted to an internal pressure of 20 MPa.

For the convergence assessment for each method, the standardized SIF profile values obtained along θ will be evaluated through the mean square error and the mean percentage error, respectively defined as:

$$\overline{E} = \sqrt{\frac{\sum_{i=1}^{n}\left(K_{I,i}^{A} - K_{I,i}^{N}\right)^2}{n}} \tag{5}$$

$$E\% = \frac{\sum_{i=1}^{n}\left|K_{I,i}^{A} - K_{I,i}^{N}\right|}{n} \times 100 \tag{6}$$

where $K_{I,i}^{A}$ is the normalized mode I SIF obtained from the analytical solutions; $K_{I,i}^{N}$ is the normalized mode I SIF obtained by the numerical techniques (XFEM and FEM); n is the number of values obtained along the semi elliptical profile, i.e., along θ. Also, K_I^{norm} values will be evaluated considering the percentage error on $\theta = 0°$ and $\theta = 90°$, because of the importance of the SIF values at this parametric angular location for structural integrity assessment.

For the hollow cylinder case, the FEM and XFEM models will be developed considering a complete model and a surface-based tie constraint model, as shown in Figure 3. Surface-based tie constraint ties two surfaces together for the duration of the simulation, constraining each of the nodes on the slave surface to have the same motion as the master surface to which it is closest (Dassault Sytèmes, 2012). This technique available in ABAQUS® is used for mesh refinement purposes, but in this case will be used to reduce computational cost of the models. This technique has been used successfully by Tipple and Thorwald (2012). The complete models will be called CM and the surface-base tie constraint, TC.

Considering mesh structuring technique on the crack location, for both the plate and hollow cylinder, two techniques will be considered for the XFEM models. The first technique was cited by Levén and Rickert (2012) and will be called here STRUC-1. The second technique was cited by Qian et al. (2016) and will be called STRUC-2. Both mesh structuring techniques are shown in Figure 4, as well as the technique used for the FEM model, which is known as the spider-web mesh.

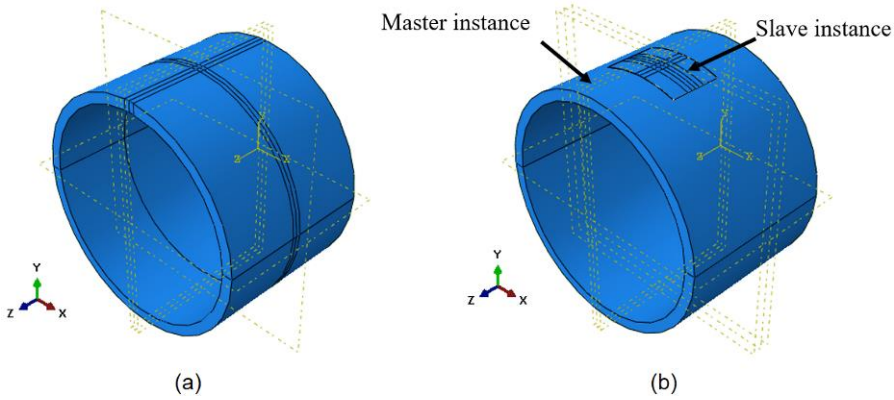

Figure 3. Hollow cylinder (a) complete model; (b) surface-based tie constraint model.

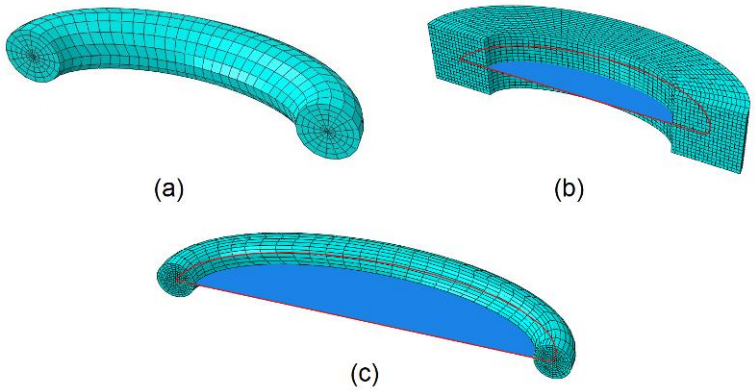

Figure 4. Mesh structuring technique around semi elliptical crack. (a) FEM model (spider-web mesh); (b) XFEM model (STRUC-1); (c) XFEM model (STRUC-2).

3. RESULTS AND DISCUSSION

3.1 Plate with a centered surface Crack

Table 2 shows information from meshes of the numerical techniques used for this case.

The FEM model used C3D15 elements for the crack tip (a 15-node quadratic triangular prism element) and C3D20R elements at the rest of the structure (a 20-node quadratic hexahedral brick element with reduced integration), resulting in a 48,284 elements mesh. Fig. 5 shows the details of this model. Figure 5(c) shows the unstructured deformed mesh necessary for the crack topology agreement in fracture FEM models.

The XFEM-1 and XFEM-2 models used only C3D8R (an 8-node quadratic hexahedral brick element with reduced integration) and resulted in a 77,460 and 43,692 elements mesh, respectively. Fig. 6 and Fig. 7 shows details of these models. In Fig. 6(c) and Fig. 7(c) is possible to see the structured mesh around the crack tips for both mesh structuring techniques here considered, as XFEM does not require mesh to be agreed with crack topology.

Table 2. Mesh information for the plate with a centered surface crack.

Model	Mesh structuring technique	Type of elements	Element order	Number of elements	Number of nodes
FEM	Spider-web	C3D15 + C3D20R	Quadratic	48,284	211,091
XFEM-1	STRUC-1	C3D8R	Linear	77,460	86,064
XFEM-2	STRUC-2	C3D8R	Linear	43,692	48,785

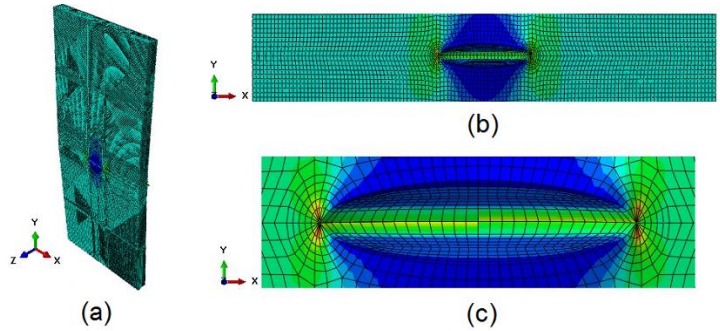

Figure 5. FEM model for the plate with a centered surface crack. (a) meshed deformed model; (b) detailed mesh in the deformed crack region; (c) zoom at the crack opening.

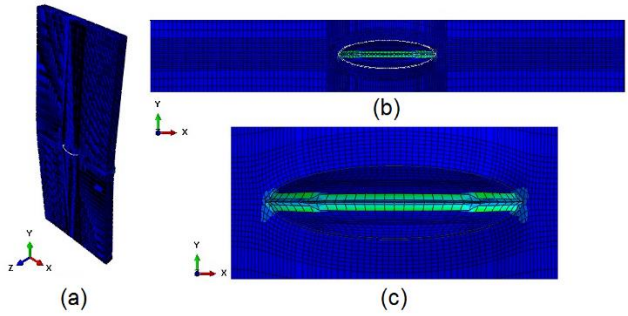

Figure 6. XFEM-1 model for the plate with a centered surface crack. (a) meshed deformed model; (b) detailed mesh in the deformed crack region; (c) zoom at the crack opening.

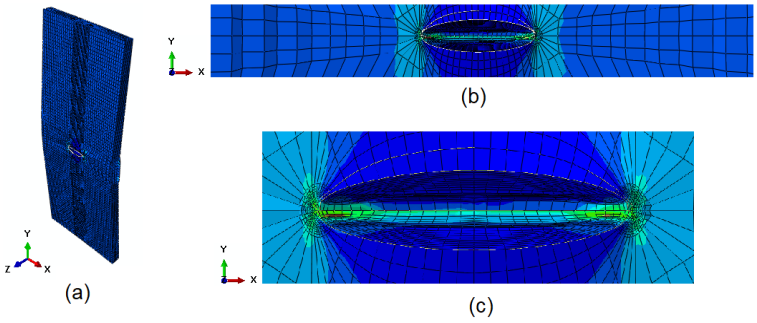

Figure 7. XFEM-2 model for the plate with a centered surface crack. (a) meshed deformed model; (b) detailed mesh in the deformed crack region; (c) zoom at the crack opening.

In Figure 8 only half the K_I^{norm} profile along the parametric angle ($0° \leq \theta \leq 90°$) is shown for the analytical and numerical solutions. The mean square and percentage errors, and the values at θ = 0° and θ = 90° K_I^{norm} percentage errors for each model are shown in Tab. 3.

Table 3. Mean square and mean percentage error for the plate models.

Model	$\overline{E}$	$E\%$	$E\%(\theta = 0°)$	$E\%(\theta = 90°)$
FEM	0.018	1.68 %	2,59 %	2,03 %
XFEM-1	0.015	1.35 %	0,28 %	2,38 %
XFEM-2	0.068	6,74 %	6,47 %	1,71 %

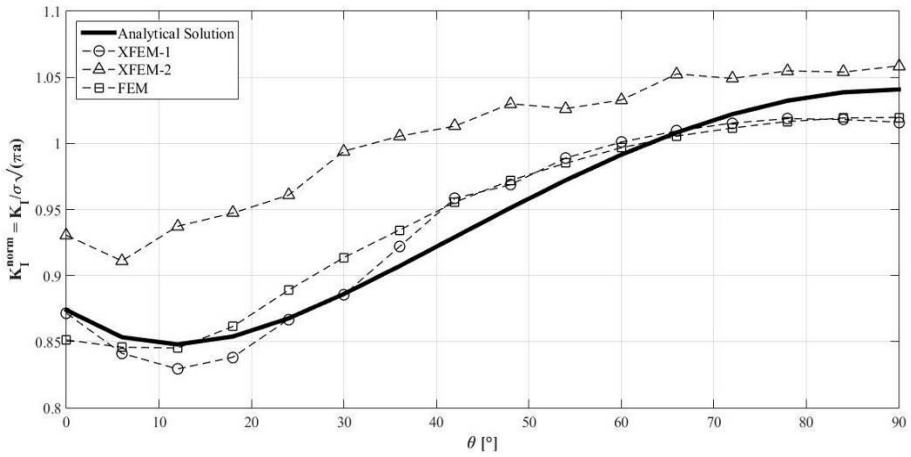

Figure 8. Normalized mode I SIF profile along parametric angle for the plate with a centered surface crack.

It is noticeable a small oscillation in the XFEM-1 K_I^{norm} profile an even greater oscillation on the XFEM-2 model when compared to the FEM K_I^{norm} profile. This effect was already reported by Levén and Rickert (2012) to be expected with the use of XFEM for SIF estimation. Qian, et al. (2016) also observed such effect and assigned it to be caused by the limitation of the enrichment function and limitations of the energy release integral implementation and extraction domains.

Both numerical techniques displayed good results for the plate geometry considering the profile evaluated. The XFEM-1 model particularly exhibited a slightly better K_I^{norm} profile compared to the FEM model and approximate better for the K_I^{norm} value at θ = 0°, which is assigned to the STRUC-1 mesh structuring technique. The XFEM-2 model, however, displayed poor results considering the entire profile, which is assigned to the STRUC-2 mesh structuring technique, but was able to approximate better for the K_I^{norm} at θ = 90°. A slight deviation of K_I^{norm} at θ = 90° could be observed for the XFEM-1 model. This deviation has also been observed by Levén and Rickert (2012).

3.2 Hollow Cylinder with Surface Crack on Outside Surface, Axial Direction

Table 4 shows information from meshes of both numerical techniques used for this case.

The FEM-CM and FEM-TC model used C3D15 elements for the crack tip (a 15-node quadratic triangular prism element) and C3D20R elements at the rest of the structure (a 20-node quadratic hexahedral brick element with reduced integration), resulting in an 188,028 and 28,430 elements mesh, respectively. Fig. 9 and Fig. 10 shows the details of these models. Figure 9(c) and Fig. 10(c) shows the unstructured deformed mesh necessary for the crack topology agreement in fracture FEM models.

The XFEM-CM-1, XFEM-CM-2, XFEM-TC-1 and XFEM-TC-2 models used only C3D8R (an 8-node quadratic hexahedral brick with element reduced integration) and resulted in an 89,176, 296,484, 32,280, 43,322 elements mesh, respectively. Fig. 11, Fig. 12, Fig. 13 and Fig. 14 shows details of these models. In Fig. 11(c), Fig. 12(c), Fig. 13(c) and Fig. 14(c) is possible to see the structured mesh around the crack tips.

Table 4. Mesh information for the hollow cylinder with a surface crack on outside surface, axial direction.

Model	Mesh structuring technique	Type of elements	Element order	Number of elements	Number of nodes
FEM-CM	Spider-web	C3D15 + C3D20R	Quadratic	188,028	837,854
FEM-TC	Spider-web	C3D15 + C3D20R	Quadratic	28,430	137,161
XFEM-CM-1	STRUC-1	C3D8R	Linear	89,176	95,708
XFEM-CM-2	STRUC-2	C3D8R	Linear	296,484	329,718
XFEM-TC-1	STRUC-1	C3D8R	Linear	32,280	39,442
XFEM-TC-2	STRUC-2	C3D8R	Linear	43,322	50,215

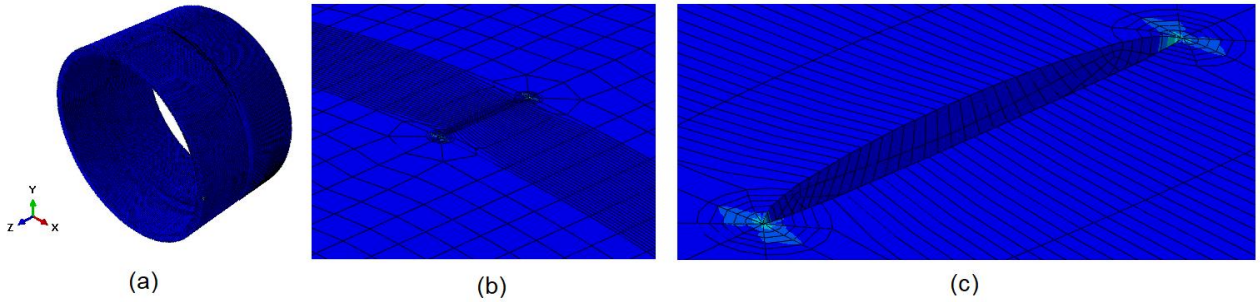

Figure 9. FEM-CM model for the hollow cylinder with a surface crack on outside surface, axial direction. (a) meshed deformed model; (b) detailed mesh in the deformed crack region; (c) zoom at the crack opening.

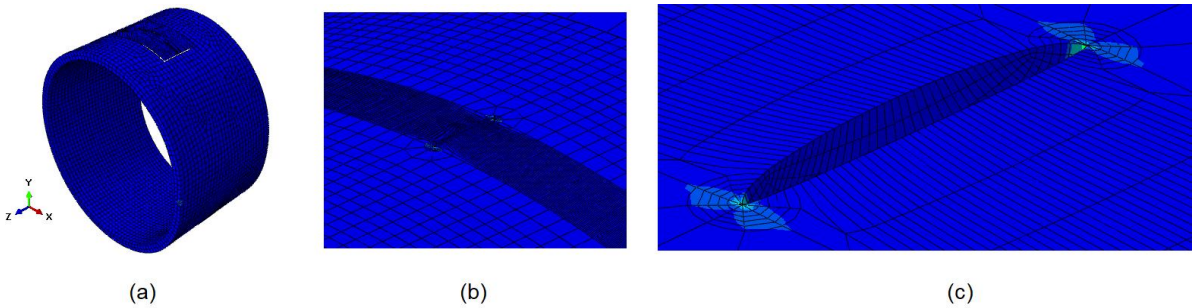

Figure 10. FEM-TC model for the hollow cylinder with a surface crack on outside surface, axial direction. (a) meshed deformed model; (b) detailed mesh in the deformed crack region; (c) zoom at the crack opening.

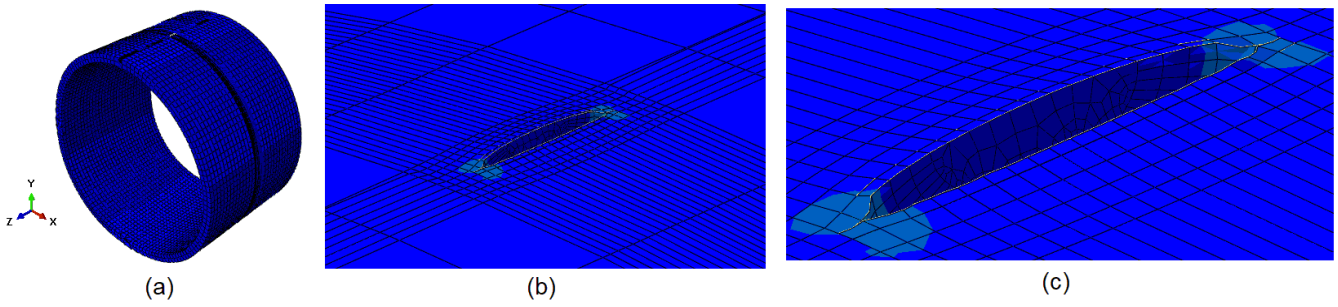

Figure 11. XFEM-CM-1 model for the hollow cylinder with a surface crack on outside surface, axial direction. (a) meshed deformed model; (b) detailed mesh in the deformed crack region; (c) zoom at the crack opening.

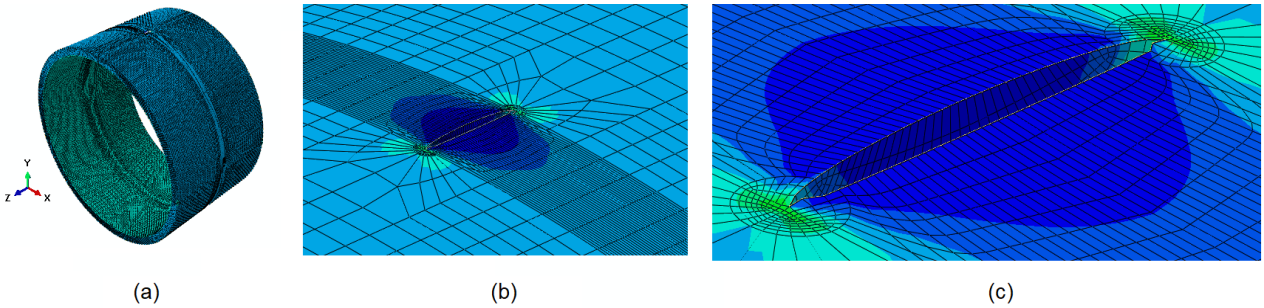

Figure 12. XFEM-CM-2 model for the hollow cylinder with a surface crack on outside surface, axial direction. (a) meshed deformed model; (b) detailed mesh in the deformed crack region; (c) zoom at the crack opening.

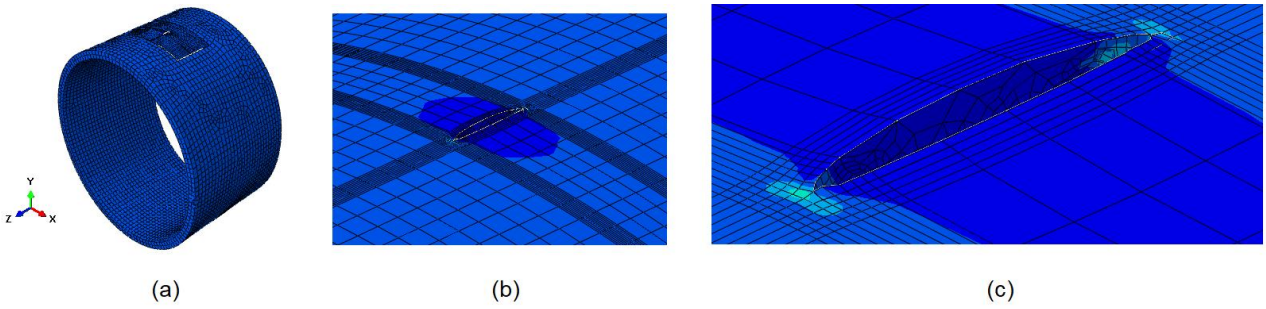

Figure 13. XFEM-TC-1 model for the hollow cylinder with a surface crack on outside surface, axial direction. (a) meshed deformed model; (b) detailed mesh in the deformed crack region; (c) zoom at the crack opening.

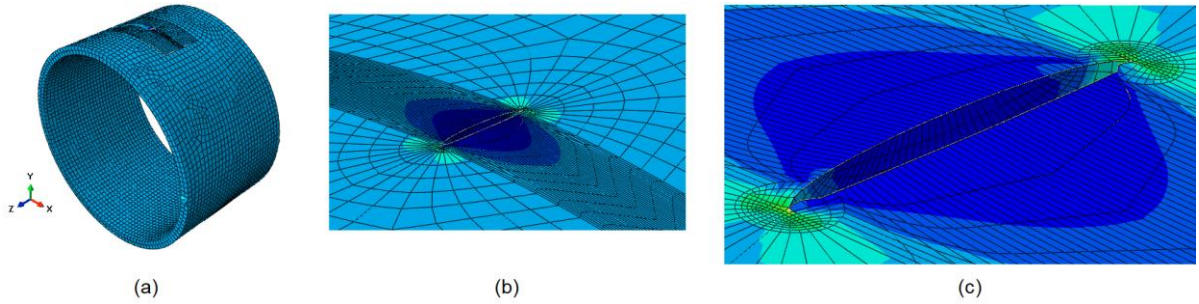

Figure 14. XFEM-TC-2 model for the hollow cylinder with a surface crack on outside surface, axial direction. (a) meshed deformed model; (b) detailed mesh in the deformed crack region; (c) zoom at the crack opening.

In Figure 15 all the K_I^{norm} profiles obtained with all the XFEM models are shown. Fig. 16 compares the K_I^{norm} profile of the XFEM-CM-1, FEM-CM and FEM-TC models. Fig. 17 shows the K_I^{norm} profiles for the XFEM-CM-2 in comparison to the FEM-CM and FEM-TC models profiles. In Fig. 18 it is shown the K_I^{norm} profile obtained for the XFEM-TC-1 model, same comparison. Fig. 19 shows the same comparison for the XFEM-TC-2 model. The mean square and percentage errors, and the K_I^{norm} values at $\theta = 0°$ and $\theta = 90°$ values percentage errors for each model are shown in Tab. 4.

Considering the two types of models used, the surface-based tie constraint provided better results than the use of complete models, regardless the numerical technique used, FEM or XFEM. The FEM-TC displayed lower mean square and mean percentage errors than the FEM-CM, and the XFEM-TC-1 and XFEM-TC-2 displayed lower mean square and mean percentage errors than the XFEM-CM-1 and XFEM-CM-2, respectively.

Regarding the two mesh structuring techniques considered, STRUC-2 provided excellent results considering the reduction of oscillation, which was not observed for STRUC-1. XFEM-CM-2 and XFEM-TC-2 models displayed far better results than XFEM-CM-1 and XFEM-TC-1, respectively, reducing the mean square and mean percentage errors. Some minor oscillation was still observed for models with STRUC-2 mesh structuring technique in $\theta = 0°$ and near this parametric angular location.

Table 4. Mean square and mean percentage error for the hollow cylinder models.

Model	$\overline{E}$	$E\%$	$E\%(\theta = 0°)$	$E\%(\theta = 90°)$
FEM-CM	0,039	4,65 %	8,59 %	4,91 %
FEM-TC	0,019	2,02 %	2,17 %	1,23 %
XFEM-CM-1	0,13	13,19 %	29,12 %	8,37 %
XFEM-CM-2	0,036	3,92%	6,02 %	0,57 %
XFEM-TC-1	0,053	4,41 %	13,21 %	1,42 %
XFEM-TC-2	0,029	2,91 %	8,29 %	1,65 %

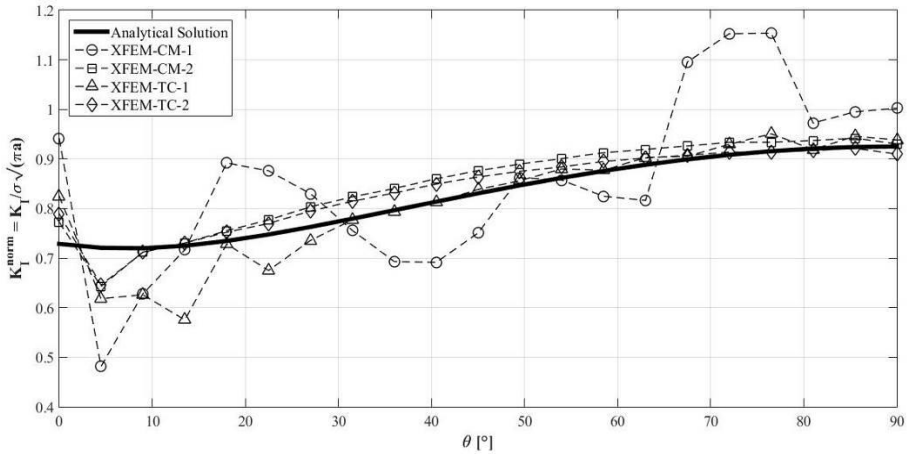

Figure 15. Normalized mode I SIF profile along parametric angle of all XFEM models for the hollow cylinder with a surface crack on outside surface, axial direction.

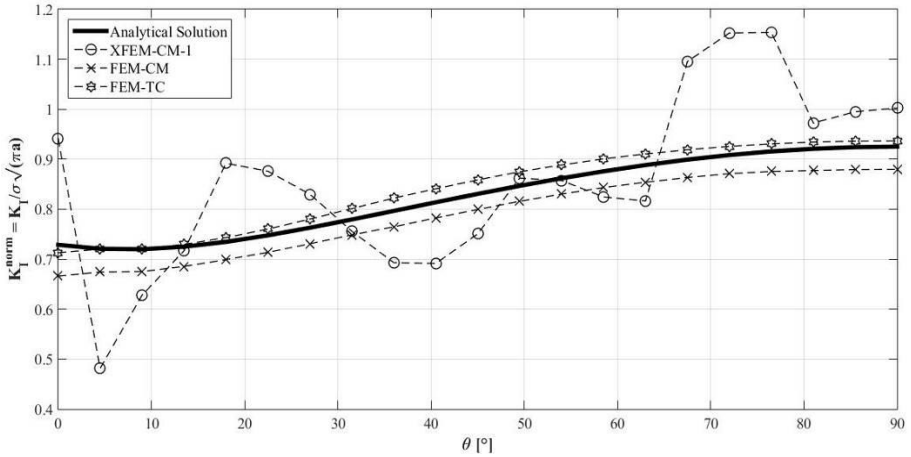

Figure 16. Normalized mode I SIF profile along parametric angle of all XFEM-CM-1, FEM-CM and FEM-TC models for the hollow cylinder with a surface crack on outside surface, axial direction.

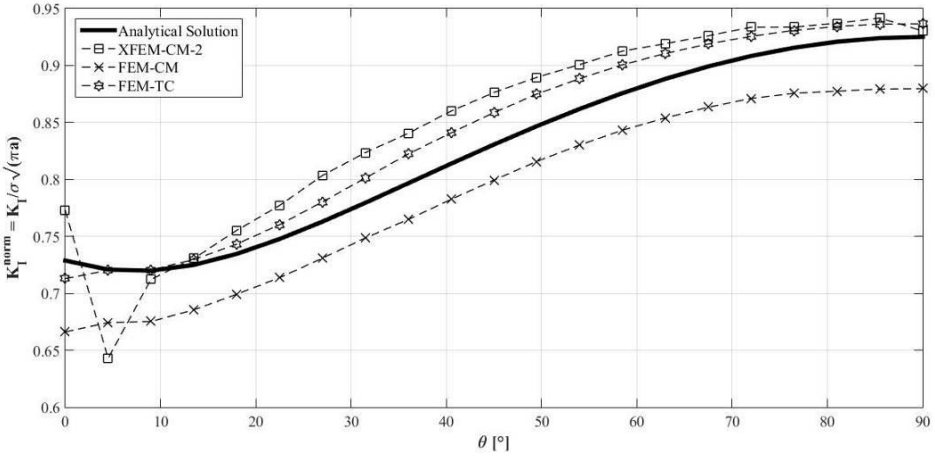

Figure 17. Normalized mode I SIF profile along parametric angle of all XFEM-CM-2, FEM-CM and FEM-TC models for the hollow cylinder with a surface crack on outside surface, axial direction.

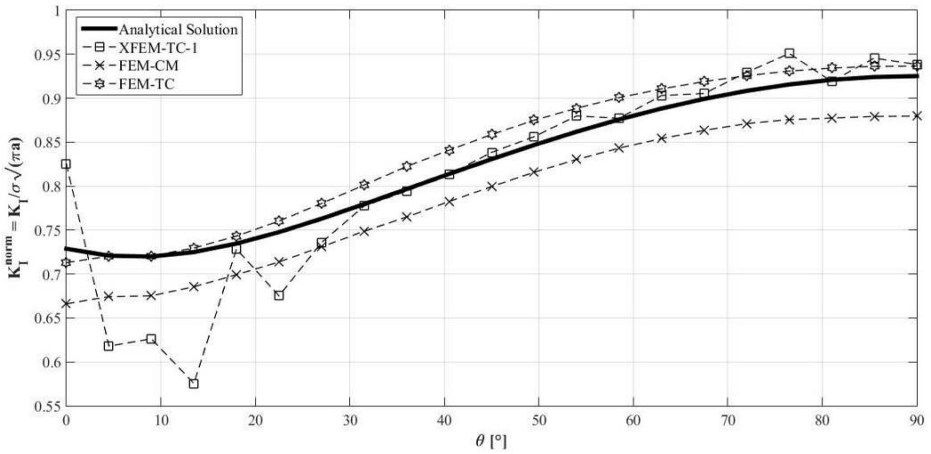

Figure 18. Normalized mode I SIF profile along parametric angle of all XFEM-TC-1, FEM-CM and FEM-TC models for the hollow cylinder with a surface crack on outside surface, axial direction.

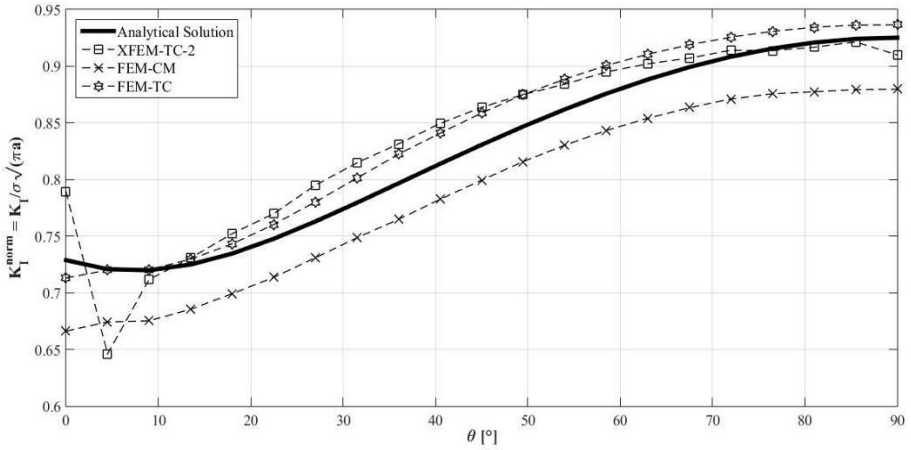

Figure 19. Normalized mode I SIF profile along parametric angle of all XFEM-TC-2, FEM-CM and FEM-TC models for the hollow cylinder with a surface crack on outside surface, axial direction.

The combination of the models used with the mesh structuring technique was fundamental for achieving good results when compared to analytical solution. XFEM-TC-2 was the best model developed between the XFEM models, although the FEM-TC model agreed more to the analytical solution.

For the parametric angular locations of interests for structural integrity assessment, the FEM-TC offered better results for the K_I^{norm} at θ = 0°. At θ = 90°, it is observed a more intense deviation of K_I^{norm} for the XFEM hollow cylinder models when compared to the XFEM plate models. This more intense deviation is the reason why XFEM-CM-2 model displayed better K_I^{norm} agreement than FEM-TC.

4. CONCLUSIONS

As concluding remarks regarding the use of XFEM for SIF estimation for a surface crack on a plate:

- STRUC-1 (Levén and Rickert, 2012) offered better results for mesh structuring around crack location than STRUC-2 (Qian et al., 2016);
- Oscillation of the K_I^{norm} profile was observed for both XFEM models developed, but the STRUC-1 mesh structuring technique proved to be able to minimize such effect when compared to STRUC-2;
- Using STRUC-1 for XFEM plate model provided better results considering K_I^{norm} profile.
- Sligth deviation of K_I^{norm} at θ = 90° should be investigated to improve results at this parametric angular location.

As concluding remarks regarding the use of XFEM for SIF estimation for a surface crack on a hollow cylinder:

- STRUC-2 (Qian et al., 2016) offered excellent results to minimize the K_I^{norm} profile oscillation, what was not observed using of STRUC-1 (Levén and Rickert, 2012);
- Using surface-based tie constraint increased the quality of results when compared to the complete models, specially when used in conjunction with STRUC-2 mesh structuring technique;
- An even high deviation of K_I^{norm} at θ = 90° was observed and this increase is due to the geometry complexity of the hollow cylinder when compared to the plate.

As general concluding remarks, XFEM displayed excellent results for both the plate and the hollow cylinder when compared to FEM, but structuring the mesh at the crack location demonstrated to be crucial to improved SIF profile estimation. Further mesh structuring techniques should be tested for the geometries here explored and other common engineering geometries.

5. ACKNOWLEDGEMENTS

The Graduate Program in Mechanical Engineering of Federal University of Campina Grande (UFCG), CAPES and CNPq Brazilian research agency for funding the project Universal (Grant 444039/2014-7).

6. REFERENCES

Belytschko, T. and Black, T., 1999. “Elastic Crack Growth in Finite Elements”. *International Journal for Numerical Methods in Engineering*, v. 620, p. 601–620.

Dassault Systèmes, 2012. “Abaqus 6.12: Analysis User’s Manual”. 22 Sep. 2017 <http://abaqus.software.polimi.it/v6.12/books/usb/default.htm>

Fleming, M., Chu, Y. A., Moran, B., Belytschko, T., 1997. “Enriched Element-Free Galerkin Methods for Crack Tip Fields”. *International Journal for Numerical Methods in Engineering*, v. 40, n. 8, p. 1483–1504.

Levén, M. and Rickert, D., 2012. *Stationary 3D Crack Analysis with Abaqus XFEM for Integrity Assessment of Subsea Equipment*. Master’s Thesis (Master in Applied Mechanics), Chalmers University of Technology, Göteborg.

Melenk, J. M. and Babuška, I., 1996. “The Partition of Unity Finite Element Method: Basic theory and applications”. *Computer Methods in Applied Mechanics and Engineering*, v. 139, n. 1–4, p. 289–314.

Möes, N., Dolbow, J. and Belytschko, T., 1999. “A Finite Element Method for Crack Growth without Remeshing”. *International Journal for Numerical Methods in Engineering*, v. 150, p. 131–150.

Newman, J. C. and Raju, I. S., 1984. “Stress Intensity Factor for Cracks in Three-Dimensional Finite Bodies Subjected to Tension and Bending Loads”. Hampton, USA: *NASA Technical Memorandum 85793*.

Qian, G., González-Albuixech, V. F., Niffenegger, M. and Giner, E., 2016. “Comparison of KI Calculation Methods”. *Engineering Fracture Mechanics*, v. 156, p. 52–67.

Sukumar, N., Moës, N., Moran, B., Belytschko, T., 2000. “Extended Finite Element Method for Three- Dimensional Crack Modelling”. *International Journal for Numerical Methods in Engineering*, v. 48, n. 11, p. 1549–1570.

Sukumar, N., Dolbow, J. E., Moës, N., 2015. "Extended Finite Element Method in Computational Fracture Mechanics: A Retrospective Examination". *International Journal of Fracture*, v. 196, n. 1–2, p. 189–206.

The British Standards Institution, 2013. "BS 7910: Guide to Methods for Assessing the Acceptability of Flaws in Metallic Structures". 3 ed. London, UK: BSI Standards Limited, 478 p.

Tipple, C., Thorwald, G., 2012. "Using the Failure Assessment Diagram Method with Fatigue Crack Growth to Determine Leak-before-Rupture". In *Proceedings of the SIMULIA Customer Conference*. Providence, Rhode Island, USA.

7. RESPONSIBILITY NOTICE

The author(s) is (are) the only responsible for the printed material included in this paper.